Chemical Engineering Science 119 (2014) 99–108

Contents lists available at ScienceDirect

Chemical Engineering Science

journal homepage: www.elsevier.com/locate/ces

# Control of incident irradiance on a batch operated flat-plate photobioreactor

Razmig Kandilian, Tsu-Chin Tsao, Laurent Pilon *

*Mechanical and Aerospace Engineering Department, Henry Samueli School of Engineering and Applied Science, University of California, Los Angeles, Los Angeles, CA 90095, USA*

## HIGHLIGHTS

- *Nannochloropsis oculata* was grown in a flat-plate photobioreactor (PBR) operated in batch mode.
- A model-free optimal search rapidly determined the optimum average fluence rate.
- Feed-forward inversion control continuously adjusted incident irradiance on the PBR.
- Controlling incident irradiance on PBRs enhanced productivity and reduced lag time.
- The procedure presented can be applied to any microorganism species or PBR design.

## ARTICLE INFO

*Article history:*
Received 21 May 2014
Received in revised form
15 July 2014
Accepted 26 July 2014
Available online 8 August 2014

*Keywords:*
Feed-forward control
PBR optimization
Light transfer
Nannochloropsis
Biofuels

## ABSTRACT

This study experimentally demonstrated a feed-forward inversion control scheme for maintaining an optimum incident irradiance on photobioreactors (PBRs) during batch cultivation. A data-based model-free optimization using quadratic fit was utilized to rapidly estimate the optimum average fluence rate set point value that rendered maximum microalgae growth rate. Then, the feed-forward inversion control scheme adjusted the incident irradiance with respect to the in-process measured mass concentration to maintain the optimum average fluence rate inside the PBR. Optimization of growth conditions with respect to light is of prime importance for increasing biomass and lipid productivity in microalgae cultivation. The present approach can rapidly identify the optimum average fluence rate for any given species, reduce the lag time, and increase the growth rate and productivity of microalgae. This was illustrated with *Nannochloropsis oculata* batch grown in a flat-plate PBR illuminated from both sides.


## 1. Introduction

Due to concerns over the environment and energy security, biofuels have been tipped as the next generation transportation fuel to replace gasoline and diesel derived from petroleum (IPPC, 2007). Production of first and second generation biofuels such as bioethanol from corn, soybean, sugarcane, and jatropha has been optimized and is currently profitable (Ferrell and Sarisky-Reed, 2010). However, it only accounts for 1% of the total transportation fuel production in the United States (Ferrell and Sarisky-Reed, 2010). Furthermore, it would be unsustainable if large quantities were produced (Chisti, 2007; Williams and Laurens, 2010; Ferrell and Sarisky-Reed, 2010; Chen et al., 2011a). Indeed, producing enough corn to displace 50% of the transportation fuel needs in the U.S. would require surface area eight times larger than the current U.S. arable land (Chisti, 2007; Jones and Mayfield, 2012). By contrast, estimates suggest that lipid producing microalgae would only require between 1 and 3% of the U.S. cropping area for the same outcome (Chisti, 2007). Consequently, microalgae are being considered for producing next-generation biofuels thanks to their large growth rate and large lipid content (Chisti, 2007; Williams and Laurens, 2010). However, despite its large photosynthetic efficiency, microalgae biodiesel remains approximately three times more expensive to produce than its petroleum counterpart (Jones and Mayfield, 2012). Chisti (2012) determined that the cost of production for biomass composed of 40 dry wt% lipids must be less than $0.50 for microalgal biodiesel to be economically competitive with $100 per barrel of crude oil. However, current estimates of dry biomass production costs range from $5 to $100 per kilogram (Chisti, 2012, 2013). Alternatively, Stephens et al. (2010) illustrated that biodiesel production by large-scale ($>500$ hectare), microalgae production systems may be profitable if they were also used

* Corresponding author. Tel.: +1 310 206 5598; fax: +1 310 206 4830.
*E-mail address:* pilon@seas.ucla.edu (L. Pilon).

http://dx.doi.org/10.1016/j.ces.2014.07.056
0009-2509/

for co-producing high-value products such as acid-hydrolyzed vegetable protein (HVP) or beta-carotene which can be sold for $600/kg.

Furthermore, the Energy Independence and Security Act of 2007 established the renewable fuel standards mandating 36 billion gallons of renewable biofuels to be blended with transportation fuels sold in the U.S. by year 2022 (Ferrell and Sarisky-Reed, 2010). At most 15 of the 36 billion gallons are expected to be bioethanol and the remainder is projected to come from microalgae-based biodiesel (Ferrell and Sarisky-Reed, 2010). Microalgae are also sought after for the high value chemicals and pharmaceuticals they can produce. For example, pigments such as astaxanthin and $\beta$-carotene are used as colorants or antioxidants in the food and pharmaceutical industries (Williams and Laurens, 2010). These secondary products have a much smaller market size. However, they command prices per mass three to four orders of magnitude larger than biodiesel (Williams and Laurens, 2010). In these different applications, identifying optimum growth conditions and increasing microalgae biomass productivity are essential.

Microalgae can be produced in large quantities in photobioreactors (PBRs) operated in batch or continuous mode. Batch cultivation is more widely used due to its simplicity and low cost (Chen et al., 2011b). Optimization of the light available to microorganisms in PBRs is a crucial aspect of biomass production and process productivity (Ferrell and Sarisky-Reed, 2010; Pilon et al., 2011; Carvalho et al., 2011; VanVooren et al., 2012; Pruvost and Cornet, 2012). Light is the energy source that enables these photosynthetic microorganisms to metabolize. Inadequate amount of light causes a decrease in growth and photosynthesis rates due to lack of energy necessary to fixate carbon. Similarly, exposing microalgae to excessively large irradiances causes photo-oxidative damage in photosystem II units. The cells continuously perform a damage repair cycle to repair the damaged photosystem II units (Baroli and Melis, 1996; Neidhardt et al., 1998). However, when the damage rate exceeds the repair rate, photoinhibition becomes apparent and the overall cell photosynthetic efficiency decreases (Baroli and Melis, 1996; Ke, 2001). Identifying the optimum level of irradiance required for maximum microalgae growth rate and maintaining an optimum fluence rate in the PBR throughout the growth phase are necessary to increase biomass productivity.

This study aims to develop a versatile and robust scheme to control the incident irradiance on PBRs for maximizing microalgae growth rate and biomass productivity. The method should be able to rapidly identify the optimum light conditions. It should also be applicable to any species and/or PBR without prior knowledge of the culture growth kinetics.

## 2. Background

### 2.1. Radiative transfer model

In order to predict the light intensity distribution in PBRs, it is necessary to solve the steady-state radiative transfer equation (RTE) in homogeneous absorbing, scattering, but non-emitting media given by (Modest, 2003)

$$\hat{s}\cdot\nabla I_\lambda = -\kappa_\lambda I_\lambda(\hat{r},\hat{s}) - \sigma_{s,\lambda} I_\lambda(\hat{r},\hat{s}) + \frac{\sigma_{s,\lambda}}{4\pi}\int_{4\pi} I_\lambda(\hat{r},\hat{s}_i)\Phi_\lambda(\hat{s}_i,\hat{s})\, d\Omega_i \tag{1}$$

where $I_\lambda(\hat{r},\hat{s})$ is the spectral radiation intensity in direction $\hat{s}$ at location $\hat{r}$ (in W/m$^2$ nm sr) while $\kappa_\lambda$ and $\sigma_{s,\lambda}$ are the absorption and single scattering coefficients (in 1/m), respectively. The scattering phase function $\Phi_\lambda(\hat{s}_i,\hat{s})$ represents the probability that radiation traveling in the solid angle $d\Omega_i$ around direction $\hat{s}_i$ will be scattered into the solid angle $d\Omega$ around direction $\hat{s}$. The local spectral fluence rate $G_\lambda(\hat{r})$ and the fluence rate $G_{PAR}(\hat{r})$ averaged over the photosynthetically active radiation (PAR) region, defined as the spectral region between 400 and 700 nm (McCree, 1981), at location $\hat{r}$ are defined, respectively, as (Modest, 2003)

$$G_\lambda(\hat{r}) = \int_{4\pi} I_\lambda(\hat{r},\hat{s})\, d\Omega \quad \text{and} \quad G_{PAR}(\hat{r}) = \int_{PAR} G_\lambda(\hat{r})\, d\lambda \tag{2}$$

Several methods of solution for the RTE exist (Pilon et al., 2011; Dauchet et al., 2013; Lee et al., 2014; Kong and Vigil, 2014). Pottier et al. (2005) derived an analytical solution to the one-dimensional RTE using the Schuster–Schwarzschild two-flux approximation in order to model light transfer through a well-mixed algal cultures in vertical flat-plate PBRs. The local spectral fluence rate $G_\lambda(z)$ in such PBRs with (i) normally incident light at $z=0$ and (ii) perfectly transmitting back wall at $z=L$ was given by Pottier et al. (2005) as

$$\frac{G_\lambda(z)}{G_{in,\lambda}} = 2\frac{(1+\alpha_\lambda)e^{\delta_\lambda X(L-z)} - (1-\alpha_\lambda)e^{-\delta_\lambda X(L-z)}}{(1+\alpha_\lambda)^2 e^{\delta_\lambda XL} - (1-\alpha_\lambda)^2 e^{-\delta_\lambda XL}} \tag{3}$$

where $G_{in,\lambda}$ is the spectral irradiance incident on the surface of the PBR. Here, $X$ is the dry mass concentration of microalgae (in kg/m$^3$) and $L$ is the PBR thickness (in m). The coefficients $\alpha_\lambda$ and $\delta_\lambda$ are expressed as (Pottier et al., 2005)

$$\alpha_\lambda = \sqrt{\frac{\overline{A}_{abs,\lambda}}{\overline{A}_{abs,\lambda} + 2b_\lambda \overline{S}_{sca,\lambda}}} \quad \text{and} \quad \delta_\lambda = \sqrt{\overline{A}_{abs,\lambda}(\overline{A}_{abs,\lambda} + 2b_\lambda \overline{S}_{sca,\lambda})} \tag{4}$$

where $\overline{A}_{abs,\lambda}$ and $\overline{S}_{sca,\lambda}$ (in m$^2$/kg) are the average mass absorption and scattering cross-sections of the microalgae suspension, respectively. They are related to the absorption and scattering coefficients by (Pilon et al., 2011)

$$\kappa_\lambda = \overline{A}_{abs,\lambda} X \quad \text{and} \quad \sigma_{s,\lambda} = \overline{S}_{sca,\lambda} X \tag{5}$$

In addition, $b_\lambda$ is the backward scattering fraction defined, for axisymmetric scattering, as (Cornet and Albiol, 2000; Pottier et al., 2005)

$$b_\lambda = \frac{1}{2}\int_{\pi/2}^{\pi} \Phi_\lambda(\theta)\sin\theta\, d\theta \tag{6}$$

where $\theta$ is the scattering angle between directions $\hat{s}_i$ and $\hat{s}$.

Similarly, the volume-averaged fluence rate $G_{ave}$ in a one-dimensional PBR of thickness $L$ over the PAR region can be estimated from the local spectral fluence rate as (Molina Grima et al., 1996; Acien Fernandez et al., 1997)

$$G_{ave} = \frac{1}{L}\int_0^L G_{PAR}(z)\, dz \tag{7}$$

### 2.2. Growth model

The time rate of change of the microorganism mass concentration $X(t)$ can be predicted by the exponential growth equation:

$$\frac{dX}{dt} = \mu X \tag{8}$$

where $\mu$ is the specific growth rate expressed in h$^{-1}$. Despite the presence of fluence rate gradient in the PBR, growth kinetics models often use the average fluence rate $G_{ave}$ (Sukenik et al., 1991; Molina Grima et al., 1996; Acien Fernandez et al., 1997; Chen et al., 2011b). This approach is valid for optically thin PBRs where the fluence rate does not significantly vary within the PBR (Fernandes et al., 2010; Lee et al., 2014; Kong and Vigil, 2014). A more general approach is to relate the growth rate $\mu(z)$ to the local fluence rate $G_{PAR}(z)$ and average it over the volume of the PBR (Cornet and Dussap, 2009; Murphy and Berberoğlu, 2011; Takache et al., 2012; Lee et al., 2014).

Finally, the daily volumetric productivity $P_v$ (in kg/m$^3$ day) and the daily areal productivity $P_A$ (in kg/m$^2$ day) of a PBR, defined as the average biomass produced daily per unit volume and per unit

surface area of PBR exposed to the light source, can be defined as

$$P_v = \frac{X_f - X_0}{\tau} \quad \text{and} \quad P_A = P_v \frac{L}{2} \tag{9}$$

where $\tau$ (in days) is the duration needed to reach the saturation mass concentration $X_f$ from an initial mass concentration $X_0$.

### 2.3. Nannochloropsis oculata

In the present study, the marine eustigmatophyceae *N. oculata* was selected for its relatively large biomass growth rate and its large lipid content. In fact, it can contain up to 45% of triglyceride lipids by dry weight (VanVooren et al., 2012; Kandilian et al., 2014) and its daily biomass productivity can reach up to 3 kg/m$^3$ day (Briassoulis et al., 2010; Chen et al., 2011a). It can also be cultivated in seawater thus eliminating competition for freshwater for human consumption or agricultural use.

Various studies have aimed at finding the optimum operating conditions for growing *N. oculata* In closed PBRs in batch mode. For example, Chiu et al. (2009) grew *N. oculata* in modified f/2 medium in batch mode in a vertical tubular PBR 7 cm in diameter exposed to 300 μmol$_{h\nu}$/m$^2$ s fluorescent light. The PBR was sparged with air or with 2 vol.% $CO_2$ in air mixture and the biomass concentration reached a maximum of 0.26 kg/m$^3$ and 1.28 kg/m$^3$, respectively. In addition, *N. oculata* cultures aerated with $CO_2$ concentrations larger than 5 vol% did not show any significant growth (Chiu et al., 2009). Spolaore et al. (2006) estimated the optimum conditions based on response surface optimization method for *N. oculata* grown in batch mode in a 2.5 l bubble column PBR with f/2 medium. These conditions were 21 °C, pH of 8.4, and incident irradiance of 52 μmol$_{h\nu}$/m$^2$ s resulting in a maximum value of specific growth rate $\mu$ of 0.036 h$^{-1}$. Converti et al. (2009) reported a maximum specific growth rate $\mu$ of 0.005 h$^{-1}$ for *N. oculata* cultivated in f/2 medium in 2 l flasks injected with 0.03 vol.% $CO_2$/air mixture exposed to incident irradiance of 70 μmol$_{h\nu}$/m$^2$ s at 20 °C. These studies demonstrate that for a given microalgae species and strain, PBR geometry, temperature, nutrient availability, and spectral light quality determine the optimum average fluence rate. The latter must be experimentally identified in order to maintain optimum conditions in the PBR and maximize its productivity.

### 2.4. Microalgae cultivation techniques

Light is one of the main limiting factors of microalgae cultivation and growth kinetics models are often used to predict the optimal operating conditions for maximum biomass or lipid productivity (Cornet and Dussap, 2009; Chen et al., 2011a; Takache et al., 2012). In fact, optimum cultivation conditions depend on microalgae species, strain, growth media, and PBR geometry (Sukenik et al., 1991; Acien Fernandez et al., 1997; Barbosa et al., 2003; Williams and Laurens, 2010). These conditions are unique for each cultivation system and can only be reliably obtained experimentally. Accurate estimation of the optimum average fluence rate is essential for optimizing PBR productivity.

Furthermore, the average fluence rate in the PBR decreases as the microalgae mass concentration increases. Therefore, to maintain a constant average fluence rate in the PBR throughout the duration of the cultivation, one must keep the cell concentration constant by diluting the culture (continuous mode) or by increasing the incident irradiance over time (batch mode). Several cultivation techniques such as the acceleration-stat and the lumostat have been developed to address this problem. For example, the aim of the acceleration-stat cultivation is to maintain a pseudo-steady state in the PBR by controlling the biomass concentration. Barbosa et al. (2003) cultivated *Dunaliella tertiolecta* in a 65 l bubble column PBR in continuous mode with a variable dilution rate. This method was successful at maintaining a relatively constant microalgae growth rate and PBR productivity for 500 h. Similarly, Cuaresma et al. (2011) designed a system that changed the concentration of *Chlorella sorokiniana* in real time in a flat-plate PBR to maintain a predetermined optimal optical transmittance. The authors simulated diurnal light conditions using a LED panel to demonstrate the feasibility of such strategy.

On the other hand, the lumostat cultivation technique relies on direct adjustment of the incident irradiance to maintain a constant growth rate and productivity in a batch cultivation (Chen et al., 2011b; Cuaresma et al., 2011; Melnicki et al., 2013). Chen et al. (2011b) measured microalgae concentration every six hours and adjusted the incident irradiance according to an empirical correlation relating the cell number density and the optimum incident irradiance. The latter was determined by first performing a series of batch cultivation experiments using *Chlorella* sp. in draft-tube PBR. The authors hypothesized that batch culture's optimum average fluence rate corresponded to its maximum chl*a* concentration. After 300 h, the PBR operated with a controlled irradiance achieved a biomass concentration 25 and 74% larger than those using constant irradiances of 82 and 590 μmol$_{h\nu}$/m$^2$ s, respectively.

Similarly, Melnicki et al. (2013) grew the cyanobacteria *Cyanothece* sp. and *Synthecoccus* sp. in a 7.5 l cylindrical PBR with an inner diameter of 13.4 cm illuminated by variable intensity LEDs at wavelengths 630 and 680 nm. The PBR was equipped with light transmission sensors and could be utilized as both an acceleration-stat or a lumostat. The authors demonstrated the system's ability to maintain a pre-determined optical transmittance through the culture by feedback-control of the LED light source. The feedback control scheme was very similar to the system developed by Cuaresma et al. (2011). Note that such system is very cost prohibitive due to the necessity to custom construct a PBR to accommodate the various sensors and actuators of the control system. It is not widely available in practice.

The main shortcoming of previous studies lies in the fact that they required extensive and time consuming experiments in order to identify the optimum average fluence rate. For example, Chen et al. (2011b) performed 4 batch cultivation experiments collecting in excess of 300 data points. In addition, previous studies relied on indirect method of identifying the optimum average fluence rate (Chen et al., 2011b). For example, a batch culture's optimum average fluence rate generally does not correspond to its maximum chl*a* concentration (VanVooren et al., 2012; Kandilian et al., 2013; Heng and Pilon, 2014). Moreover, the system presented by Melnicki et al. (2013) did not feature a method for estimating the optimum average fluence rate and was very cost prohibitive.

The present study aims to develop a novel, low-cost, robust, and model-free method to estimate the optimum average fluence rate in the PBR and use feed-forward inversion control to continuously adjust the incident irradiance on the PBR operated in batch mode. Marine microalgae *N. oculata* were used to experimentally demonstrate the approach. The biomass concentration, growth rate, and productivity of the microalgae grown under controlled irradiance were compared with those grown using constant incident irradiance.

## 3. Experiments

### 3.1. Materials and methods

#### 3.1.1. Apparatus and sensors

The microalgae species *N. oculata* UTEX 2164 were purchased from UTEX, Austin, TX. They were cultivated in artificial seawater medium. The latter had the following composition: NaCl 0.31 M, $MgSO_4 \cdot 7H_2O$ 10.5 mM, KCl 8 mM, $NaNO_3$ 11.8 mM, $CaCl_2 \cdot 2H_2O$ 2 mM, $KH_2PO_4$ 0.37 mM, $NH_4Cl$ 0.5 mM, $Na_2EDTA \cdot 2H_2O$ 0.27 mM, H3BO3 1.84 mM, $FeCl_3 \cdot 6H_2O$ 0.018 mM, $MnSO_4 \cdot H_2O$ 0.097 mM, $ZnSO_4 \cdot 7H_2O$ 0.007 mM, $CoCl_2 \cdot 6H_2O$ 0.002 mM, Vitamin B12 0.1 μM.

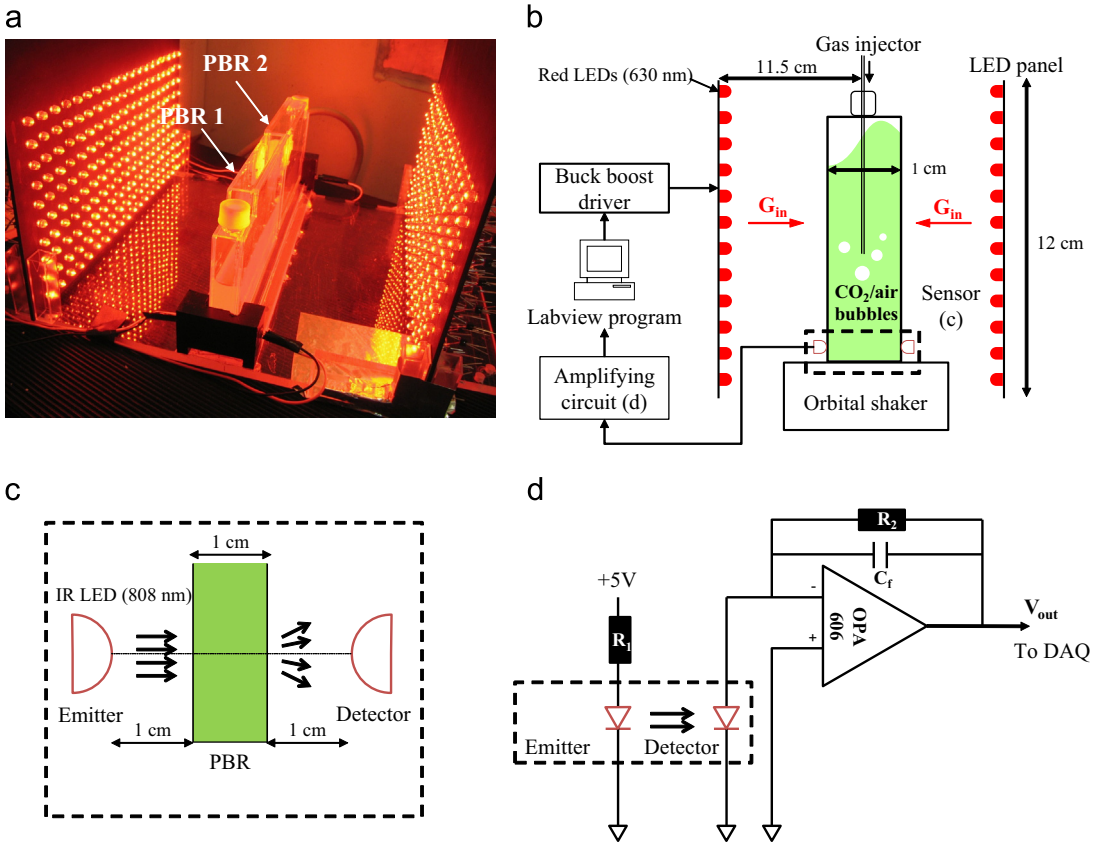


**Fig. 1.** (a) Photograph and (b) schematic of the experimental setup used in the study. (c) Mass concentration sensor with IR LED emitter and detector at 808 nm, and (d) electronic circuit used to amplify the photocurrent from the IR diode.

Figs. 1a and b show a photograph and the schematic of the experimental apparatus, respectively. It consisted of (i) a flat-plate PBR operated in batch mode, (ii) two custom made LED panels, (iii) a custom concentration sensor, and (iv) a controller. Measurements were performed in duplicates in identical PBR 1 and PBR 2 placed immediately adjacent to each other and operated simultaneously. Each PBR was a 1 cm thick flat-plate container made of acrylic filled with 70 ml of artificial seawater medium. It was continuously aerated with a mixture of air and $CO_2$ injected at a rate of 7.5 ml/min via a needle through a septum cap. The microalgae were kept in suspension using an orbital shaker rotating at 100 rpm. The pH was measured daily with a $\pm 0.01$ accuracy electrode (PHB-213 Omega Engineering, CT) and maintained between 7.7 and 8.0 by adjusting the $CO_2$ flow rate once a day as necessary. The temperature was approximately 22 °C for all experiments. Finally, all experiments started with an initial mass concentration $X_0$ of 0.02 kg/m$^3$. The LED panel consisted of 390 discrete low-power red LEDs (C503B-RAN Cree, NC) with peak emission at 630 nm and 30 nm spectral bandwidth. These LEDs were as effective in growing *N. oculata* as white fluorescent light (Kandilian et al., 2013). They were spaced 2.25 cm apart resulting in a spatial variation of less than 10% in the irradiance incident on the PBR located 11.5 cm from the LED panels. A buck-boost LED controller (LUXdrive by LEDdynamics, VT) was used to vary the intensity of the LED panels. The incident irradiance of the LED panels was adjusted by an analog voltage input to the LED controller. Fig. 1c shows a schematic of the concentration sensor assembly consisting of an infrared (IR) LED (OSRAM SFH4550, Osram-Sylvania, MA) emitting at 808 nm with a beam divergence angle of 6°. A second identical diode was placed on the other side of the PBR to sense the IR beam attenuation through the PBR. Fig. 1d shows the electrical circuit and the operational amplifier (Op-Amp) (OPA606KP Texas Instruments, TX) used to amplify the photocurrent from the detector diode. The output voltage $V_{out}$ was sent to the data acquisition system (USB-1208FS Measurement Computing Co., MA) to measure the dry mass microalgae concentration based on a calibration curve relating $V_{out}$ to $X$.

The controller input voltage $V_{ctrl}$ to the LED panel and the incident irradiance were calibrated using a LICOR LI-190 quantum sensor. Fig. 2a shows the calibration of the incident irradiance $G_{in}$ (expressed in $\mu mol_{h\nu}/m^2$ s) as a function of $V_{ctrl}$. The incident irradiance from each panel varied between 0 and 440 $\mu mol_{h\nu}/m^2$ s. The microalgae dry mass concentration $X$ was determined using a calibration curve relating $X$ to the optical density ($OD_\lambda$) of the microalgae suspension at 750 nm. Note that at 750 nm, *N. oculata* do not absorb and only scatter (Kandilian et al., 2013). The calibration curve was obtained by relating the normal-normal transmittance $T_\lambda$ and the corresponding optical density $OD_\lambda = -\ln T_\lambda$ at 750 nm for several mass concentrations of microalgae in disposable polystyrene cuvettes with 1 cm pathlength using a Fourier Transform Infrared (FTIR) spectrophotometer (ThermoNicolet Magna IR-560). The corresponding dry mass concentration $X$ was measured by filtering the cells through a previously washed and dried 0.45 nm pore size cellulose membrane filters (HAWP-04700 by Millipore, MA) followed by drying at 60 °C in a vacuum oven overnight. The dried filters with the dry cells were weighed immediately after being removed from the oven using a precision balance (model AT261 by Delta Range Factory, OH) with a 0.01 mg precision. Fig. 2b shows the calibration curve relating optical density at 750 nm $OD_{750}$ and mass concentration $X$. The resulting calibration curve was $X = 0.207 OD_{750}$.

Figs. 2c and d show the calibration curves relating the output from the Op-Amp $V_{out}$ and the microalgae concentration $X$ for PBR 1 and PBR 2 sensors, respectively. The output voltage $V_{out}$ was fitted to a natural logarithm function at low mass concentrations and to a power

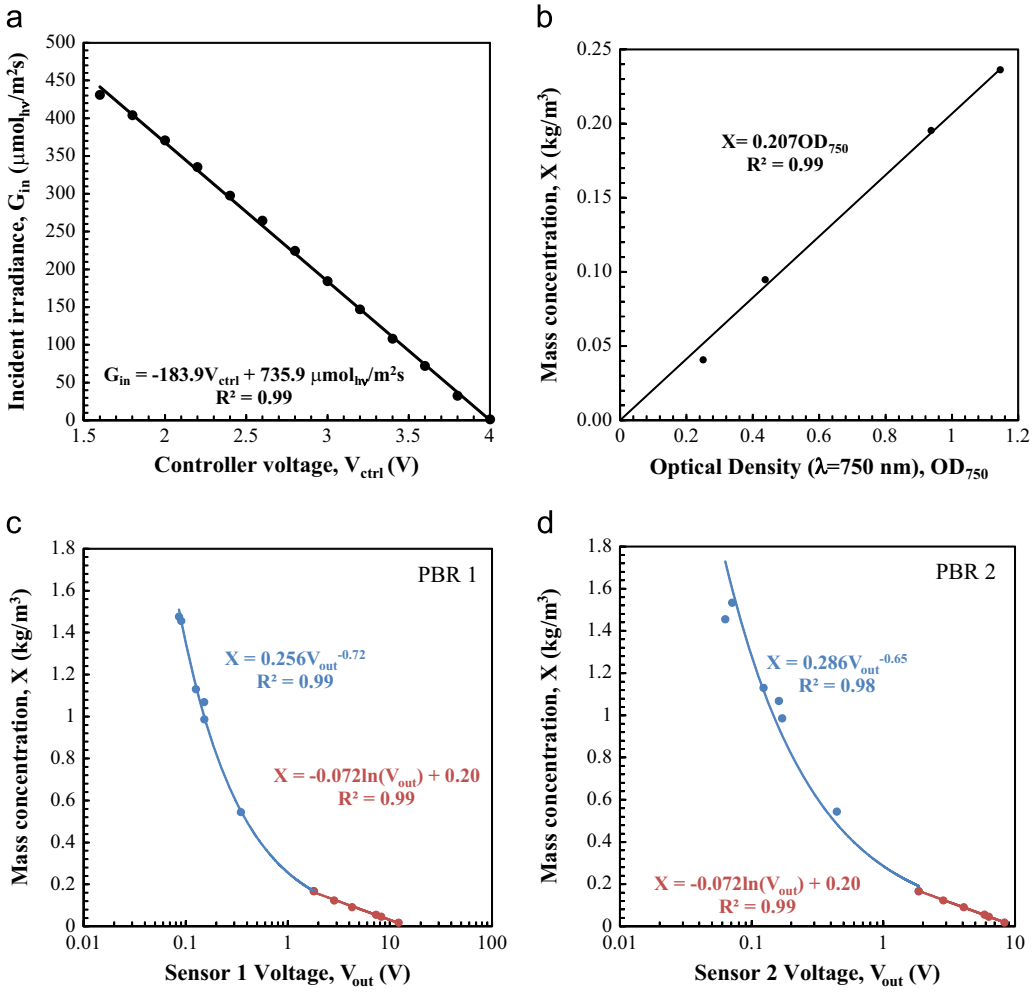


**Fig. 2.** Calibration curves for (a) the incident irradiance $G_{in}$ of the LED panel as a function of LED driver control voltage $V_{ctrl}$, and for *N. oculata* mass concentration $X(t)$ versus (b) the optical density at 750 nm $OD_{750}$, and sensor voltage $V_{out}$ for (c) PBR 1 and (d) PBR 2.

law for large concentrations. Good fits were obtained with a coefficient of determination $R^2$ larger than 0.99 for dry mass concentration $X$ in the range 0.01–1.5 kg/m$^3$. Each sensor for PBR 1 and PBR 2 was calibrated individually to ensure better accuracy and reliability of the results. The two calibration curves for PBR 1 sensor formed a continuous function while those for PBR 2 featured slight offset at $X$=0.3 kg/m$^3$. Finally, for dry mass concentration exceeding 1.5 kg/m$^3$, 0.250 ml of microalgae culture was physically sampled from each PBR and diluted by adding 2.750 ml of medium to a 1 cm pathlength polystyrene cuvette before measuring the optical density $OD_{750}$.

### 3.2. Analysis

#### 3.2.1. Light transfer model

The two-flux approximation of the RTE, given by Eq. (3), can be further simplified in the case of strongly forward scattering microalgae when $b_\lambda$ approaches 0 resulting in $\alpha_\lambda$ reaching unity. Then, the local fluence rate, for the PBR shown in Fig. 1 with irradiation incident on both sides, can be expressed as

$$G_\lambda(z) = G_{in,\lambda}[e^{-\delta_\lambda Xz} + e^{-\delta_\lambda X(L-z)}] \tag{10}$$

This expression is similar to Beer–Lambert's law (Modest, 2003). However, the arguments in the exponential functions are significantly different. In fact, Beer-Lambert's law is not appropriate for predicting the local fluence rate in a PBR due to strong forward and multiple scattering by microalgae (Berberoğlu and Pilon, 2007).

The total irradiance $G_{in}$ incident on one side of the PBR over the PAR (in W/m$^2$) can be written as

$$G_{in} = \int_{400}^{700} G_{in,\lambda}\, d\lambda = G_{in,\lambda_m} \int_{400}^{700} N_\lambda\, d\lambda \tag{11}$$

where $G_{in,\lambda_m}$ is the maximum spectral incident irradiance at wavelength $\lambda_m$ between 400 and 750 nm and $N_\lambda$ is the normalized spectral distribution of the incident irradiance. Here, $\lambda_m$ was 630 nm for the LED light source used. Combining Eqs. (7) and (10), the total irradiance $G_{in}$ on each side of the PBR to achieve a desired average fluence rate $G_{ave}$ in the PBR with microorganism concentration $X$ can be written as

$$G_{in} = G_{ave} \frac{\int_{400}^{700} N_\lambda\, d\lambda}{2\int_{400}^{700} \frac{N_\lambda}{\delta_\lambda XL}(1-e^{-\delta_\lambda XL})\, d\lambda} = \frac{G_{ave}}{f(X)} \tag{12}$$

where $f(X)$ is, for all practical purposes, a function of $X(t)$, for a given PBR description and a light source. Note that the factor 2 present in the denominator of Eq. (12) was due to the fact that irradiance was incident on both sides of the PBR. Furthermore, in the asymptotic limits of $\delta_\lambda XL \ll 1$ and $\delta_\lambda XL \gg 1$, $1/f(X)$ can be simplified as

$$\frac{1}{f(X)} = \begin{cases} \dfrac{1}{2} & \text{for } \delta_\lambda XL \ll 1 \\ \dfrac{qXL}{2} & \text{for } \delta_\lambda XL \gg 1 \end{cases} \tag{13}$$

where $q$ is a constant defined as $q = \int_{400}^{700} N_\lambda \, d\lambda / \int_{400}^{700} (N_\lambda/\delta_\lambda) \, d\lambda$. Finally, the average absorption and the scattering cross-sections $\overline{A}_{abs,\lambda}$ and $\overline{S}_{sca,\lambda}$ of *N. oculata*, needed to compute $\delta_\lambda$, were reported by Kandilian et al. (2013) between 400 and 700 nm with 1 nm spectral resolution. In addition, the scattering phase function was measured at $\lambda = 632.8$ nm and was shown to be nearly constant over the PAR region. The backward scattering coefficient $b_\lambda$ was 0.002 according to Eq. (6). Note that for $\delta_\lambda XL \ll 1$, Eq. (12) can be approximated as $G_{in} \approx \frac{1}{2} G_{ave}$. On the other hand, for $\delta_\lambda XL \gg 1$, the feed-forward gain $1/f(X)$ is bounded since $XL$ is bounded.

### 3.2.2. Control scheme

Figs. 3a and b show the proposed feed-forward inversion and optimal search diagrams, respectively. The controller consisted of the radiation transfer model [Eq. (12)] and a zero-order-hold which operated at time interval $\Delta t_1$ equals to 5 min. The controller was fed with the optimum average fluence rate $G_{peak}$ and the measured mass concentration of the microalgae $X(t)$. Then, it generated the optimum incident irradiance $G_{in}(k\Delta t_1)$ necessary to achieve $G_{peak}$ where $k\Delta t_1$ corresponded to $k^{\text{th}}$ mass concentration sampling time. Similarly, the plant model, corresponding to the PBR, consisted of the radiation transfer model [Eq. (12)], the microalgae growth kinetics model relating the average fluence rate $G_{ave}$ to the growth rate $\mu$ and the microalgae growth equation [Eq. (8)]. Note that, experimentally, the mass concentration $X(t)$ was the only plant output parameter measured for the control system. The feed-forward controller is bounded-input-bounded-output stable since the feed-forward gain $1/f(X)$ is bounded, as previously discussed. One of the benefits of using such feed-forward control in microalgae cultivation lies in the fact that it does not suffer from instabilities. However, it requires accurate modeling of the system being controlled (Svrcek et al., 2007).

Moreover, the optimum average fluence rate in the PBR $G_{peak}$ must be estimated before the beginning of the feed-forward control. It corresponded to $G_{ave}$ that yielded the largest microalgae growth rate $\mu$. To estimate $G_{peak}$, an optimal search procedure was devised to empirically correlate the average fluence rate in the PBR $G_{ave}$ to the microorganism growth rate $\mu$. Brent's method is an inverse parabolic interpolation method that estimates the abscissa corresponding to the maximum of a function (Press et al., 2007). In the optimal search diagram (Fig. 3b), the radiation transfer model [Eq. (12)] in the feed-forward controller (Fig. 3a) inverted the radiation transfer model in the plant [Eq. (12)] allowing the omission of both and facilitating the simple search method. The optimal search scheme required the input of several test values of average fluence rate $G^*_{ave}$ to determine the optimum average fluence rate $G_{peak}$ using Brent's method. The latter enabled the estimation of $G_{peak}$ without requiring a model relating incident irradiance to growth rate. The only assumption made was that the growth rate $\mu$ was a convex function of the average fluence rate $G_{ave}$. The use of such a model-free optimal search algorithm increased the versatility and the applicability of the control strategy developed to any microorganism species or to other photochemical processes.

In practice, the optimal search, illustrated in Fig. 3b, preceded the feed-forward control of incident irradiance on the PBR (Fig. 3a). First, the PBR was exposed to three different irradiances $G_{in}$ on each side, namely 30, 63, and 132 $\mu mol_{h\nu}/m^2$ s. The corresponding average fluence rate test values $G^*_{ave}$ were estimated using Eq. (12), for a duration $\Delta t_2 = 3$ hours, as 59, 125, and 265 $\mu mol_{h\nu}/m^2$ s. Note that Eq. (12) simplifies to $G_{ave} \approx 2G_{in}$ at the beginning of the growth stage, since $\delta_\lambda XL \ll 1$. This suggests that the model $f(X)$ is not necessary to determine the optimal average fluence rate $G_{peak}$. This is a great feature of the present optimal search method. However, as the mass concentration $X(t)$ increases, the condition $\delta_\lambda XL \ll 1$ is no longer valid and the feed-forward controller has to rely on $f(X)$ to set the incident irradiance $G_{in}$. Then, the control performance relies on the closeness of the model $f(X)$ to the actual system. The sensitivity analysis for the present experimental system is discussed later in Section 4.2. However, the control system is robustly stable with respect to uncertainties/modeling error of $f(X)$, since the feed-forward gain $1/f(X)$ is bounded by the linear dependency of the function $f(X)$ with respect to $X$ as the latter increases. The test values for the average fluence rate $G^*_{ave}$ were chosen to fall in the photolimited and the photoinhibited regions based on growth kinetics data reported by Huertas and Lubián (1998). Note that this was performed for convenience and it was not essential to the implementation of the optimal search. The average growth rate during each period of constant irradiance was estimated in two different ways. It was first estimated by fitting the mass concentration to Eq. (8), assuming $\mu$ to be constant and equal to $\overline{\mu}$ such that

$$X = X_0 e^{\overline{\mu} t} \tag{14}$$

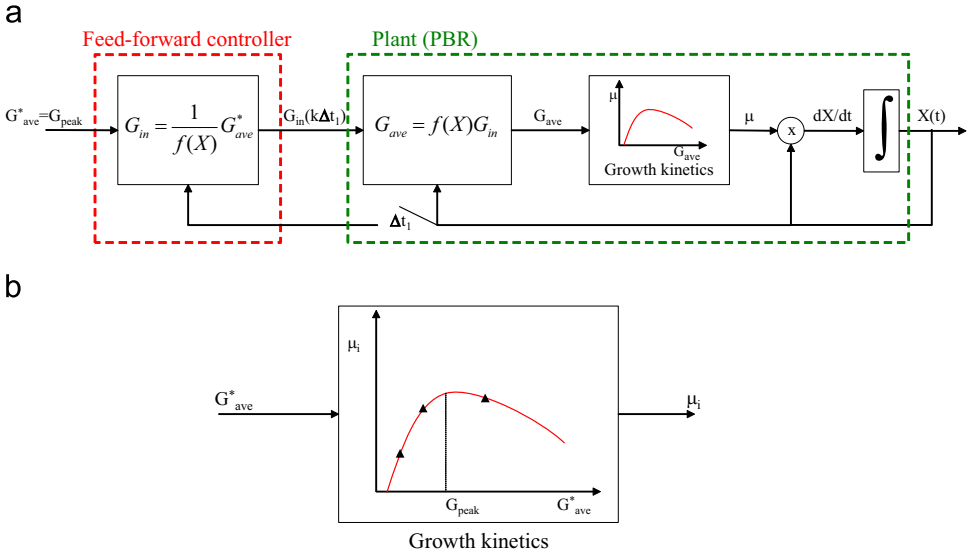


**Fig. 3.** (a) Diagram of the proposed feed-forward control scheme illustrating the controller and the plant and (b) the optimal search control diagram used to estimate $G_{peak}$ using Brent's method.

Alternatively, the growth rate was estimated at regular time intervals $\Delta t_3$ according to

$$\mu_i = \frac{1}{\Delta t_3} \ln\left[\frac{X(t_i+\Delta t_3)}{X(t_i)}\right] \quad (15)$$

Here, $\Delta t_3$ was set to 30 min to maximize signal to noise ratio. Smaller values of $\Delta t_3$ resulted in large fluctuations in $\mu_i$. Then, the average growth rate $\mu_{ave}$ for each period was estimated according to

$$\mu_{ave} = \frac{1}{n}\sum_{i=1}^{n} \mu_i \quad (16)$$

where $n$ is the number of growth rate estimates. It was equal to 24 calculated from 36 mass concentration samples $X(t_i)$ at sampling interval $\Delta t_1$ of 5 min per fitting period $\Delta t_2$ of 3 h. If the growth rate is constant during this period, $\overline{\mu}$ and $\mu_{ave}$ should be identical. The estimated average growth rates $\mu_{ave}$ or $\overline{\mu}$ for each of the three periods as functions of the corresponding average fluence rate $G_{ave}$ were then fitted to a second order polynomial. Based on Brent's method, the abscissa corresponding to the maximum of this polynomial was identified as the estimated optimum average fluence rate $G_{peak}$. Note that $\Delta t_2$ needed to be large enough so that the signal to noise ratio of the mass concentration measurements did not introduce an error in the estimated growth rate. It also had to be small enough so that changes in the operating conditions could be ignored during the optimal search period.

Once the optimum average fluence rate $G_{peak}$ was obtained, the feed-forward control scheme (Fig. 3a) adjusted the incident irradiance $G_{in}$ estimated using Eq. (12) every 5 min based on (i) the optimum average fluence rate $G_{peak}$, (ii) the mass concentration $X(t)$ measured by the sensor, and (iii) $\delta_\lambda$ calculated from the measured radiation characteristics of *N. oculata* (Kandilian et al., 2013). Note that in this experiment, the optimal search took place in the initial stage where $\delta_\lambda XL$ was significantly smaller than unity thus simplifying Eq. (12) to $G_{ave} = 2G_{in}$. Therefore, mass concentration measurements were not necessary for the radiation transfer model. If the optimal search is set active during the process, the mass concentration dependent nonlinear gain must be applied so that a varying incident irradiance $G_{in}$ will render a constant average fluence rate $G_{ave}$.

## 4. Results and discussion

### 4.1. Optimum average fluence rate

Fig. 4a shows the temporal evolution of microalgae dry mass concentration $X(t)$ for each incident irradiance $G_{in}$ on each side of the PBR for the 9 h of the optimal search. It indicates that the microalgae concentration increased under all three different values of $G_{in}$ imposed. The average growth rate $\overline{\mu}$ was retrieved by fitting the mass concentration $X(t)$ to Eq. (14).

Fig. 4b shows the growth rate $\overline{\mu}$ estimated by fitting the experimental data to Eq. (14) as a function of the duration of the fitting period ranging from 15 to 180 min for each value of $G_{in}$ imposed. The results indicate that the growth rate $\overline{\mu}$ corresponding to $G_{in} = 63$ and 132 $\mu mol_{h\nu}/m^2$ s converged to a constant value for fitting periods longer than 120 min. On the other hand, 150 min were required for the value of the growth rate $\overline{\mu}$ to converge when $G_{in}$ was 30 $\mu mol_{h\nu}/m^2$ s. This can be attributed to an initial lag period observed after transferring the culture to the PBR. Overall, the average growth rate $\overline{\mu}$ was found to be 0.008, 0.038, and 0.060 $h^{-1}$ for $G_{in}$ equal to 30, 63, and 132 $\mu mol_{h\nu}/m^2$ s, respectively. The corresponding average fluence rate $G^*_{ave}$ was estimated, based on Eq. (12), as 59, 125, and 261 $\mu mol_{h\nu}/m^2$ s, respectively.

Furthermore, Fig. 4c shows the growth rate $\mu_i$ calculated using Eq. (15) for $\Delta t_3 = 0.5$ h. The growth rates estimated by this method were noisy and scattered. However, the average growth rate $\mu_{ave}$ [Eq. (16)] for each period fell within 5% of the fitted average growth rate $\overline{\mu}$ plotted in Fig. 4b. These results provided confidence in the estimated value of the average growth rates $\overline{\mu}$ and $\mu_{ave}$.

Finally, Fig. 4d shows the function $\overline{\mu}(G^*_{ave})$ fitted to a second order polynomial. The fitting polynomial intercepted the $x$-axis (i.e., $\overline{\mu}(G^*_{ave}) = 0$) for $G^*_{ave} = 45$ $\mu mol_{h\nu}/m^2$ s corresponding to $G_{in} = 23$ $\mu mol_{h\nu}/m^2$ s for a mass concentration $X(t)$ equal to 0.02 $kg/m^3$. This offset compensated for the energy required for respiration or biomass maintenance. The ability of the model-free optimal search to identify respiration and the respiration compensation point of the species further demonstrates its versatility and value. Note that the respiration compensation point was similar in magnitude to 10 $\mu mol_{h\nu}/m^2$ s reported by Takache et al. (2012) for *Chlamydomonas reinhardtii* grown in a 1.5 l torus PBR 3 cm in thickness and illuminated from one side by 250 $\mu mol_{h\nu}/m^2$ s white LEDs. The difference in the respiration compensation point obtained from the two experiments can be attributed to the different light sources and microalgae species.

Moreover, the optimum average fluence rate $G_{peak}$ was identified as 236 $\mu mol_{h\nu}/m^2$ s by Brent's method from the three points relating the average growth rate $\overline{\mu}$ and the average fluence rate $G^*_{ave}$. This significantly differed from the values of 52 $\mu mol_{h\nu}/m^2$ s reported by Spolaore et al. (2006) and 72 $\mu mol_{h\nu}/m^2$ s used by Converti et al. (2009) for *N. oculata*. The optimum incident irradiance depends on PBR geometry, operating conditions, and the spectral quality of the light source. Differing experimental conditions may explain the differences in the reported optimum average fluence rate $G_{peak}$. Here, the latter could be achieved by imposing $G_{in} = 120$ $\mu mol_{h\nu}/m^2$ s on both sides of the PBR for initial mass concentration $X_0 = 0.02$ $kg/m^3$, according to Eq. (12).

The optimal search method implemented here can be applied to other microorganism species, PBR geometries, and operating conditions. It has the advantage of rapidly identifying the optimum incident irradiance for maximum growth rate. Furthermore, the optimal search procedure can be repeated during subsequent growth under feed-forward control to adjust for changes in the optimum average fluence rate due to changes in pigment concentration (Takache et al., 2012) and/or metabolic activity (Williams and Laurens, 2010).

### 4.2. Biomass concentration

Fig. 5a compares the temporal evolution of biomass concentration for *N. oculata* obtained under controlled incident irradiance with that obtained by exposing the PBR to a constant incident irradiance of 90 and 165 $\mu mol_{h\nu}/m^2$ s. The associated error bars were estimated from duplicate experiments and corresponded to 95% confidence interval. The microalgae culture exposed to constant irradiance of 90 $\mu mol_{h\nu}/m^2$ s featured a short lag phase and reached a saturation mass concentration of $X_f = 1.48$ $kg/m^3$ after 168 h. The culture grown under constant incident irradiance of 165 $\mu mol_{h\nu}/m^2$ s had the longest lag time due to photoinhibition. However, it reached a saturation concentration of $X_f = 2.08$ $kg/m^3$. In fact, microalgae cultures that are photolimited or exposed to lower irradiance are typically characterized by shorter lag times but reach lower saturation mass concentrations than those under higher irradiance (Chen et al., 2011a; Kandilian et al., 2013). The cultures grown in the PBR exposed to controlled incident irradiance not only had a short lag time but also reached the largest saturation mass concentration at $X_f = 2.25$ $kg/m^3$ after 185 h. In fact, the mass concentration $X(t)$ of microalgae exposed to controlled irradiance was similar to those in PBR exposed to 90 $\mu mol_{h\nu}/m^2$ s for

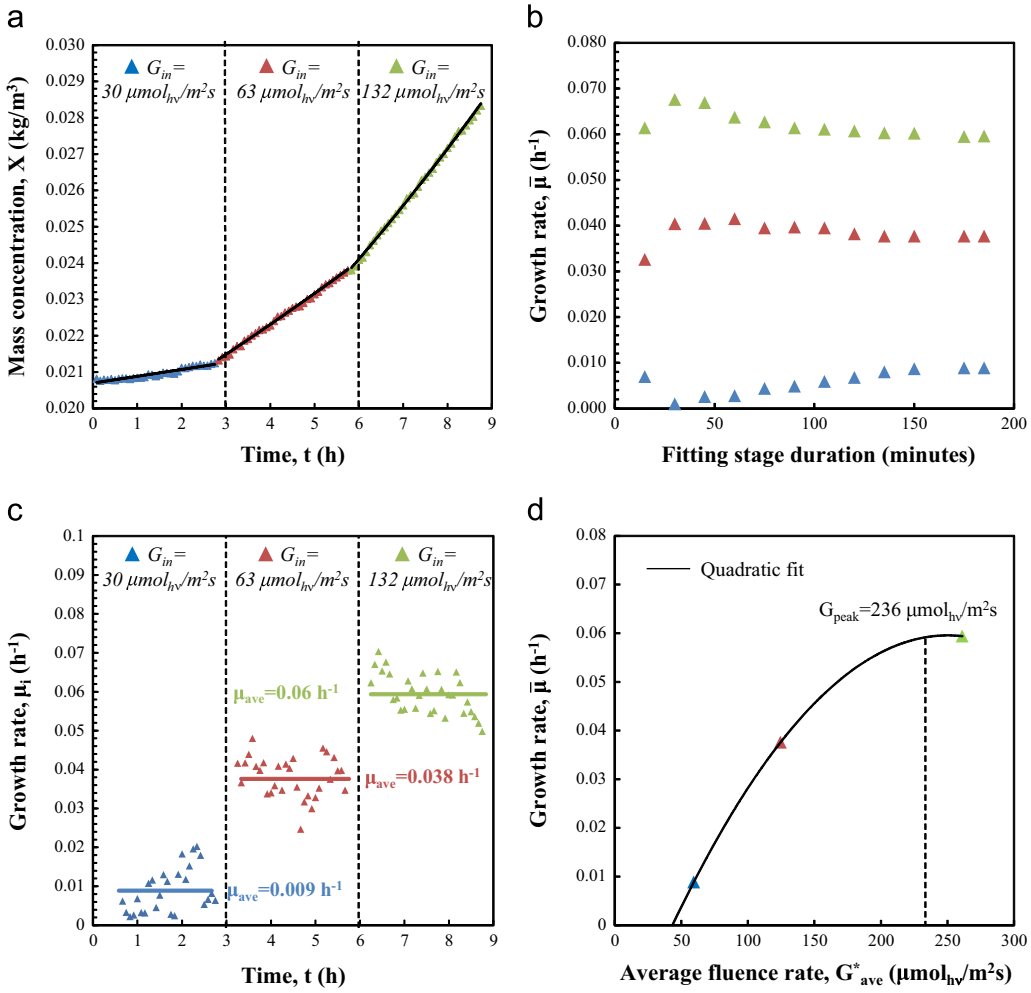


**Fig. 4.** Temporal evolution, during the optimal search of (a) the mass concentration $X(t)$, (b) the average growth rate $\overline{\mu}$ ($h^{-1}$) as a function of fitting period duration, (c) the growth rate $\mu_i(t)$ of *N. oculata*, and (d) fitted growth rate $\overline{\mu}$ versus average fluence rate $G^*_{ave}$. The optimum average fluence rate was $G_{peak} = 236\ \mu mol_{h\nu}/m^2\ s$.

approximately the first 50 h. Note that the optimal search period was relatively short and did not significantly delay the biomass growth.

Furthermore, the average volumetric batch productivity $P_v$ (Eq. (9)) over 180 h of operation was 0.326 kg/m$^3$ day when exposed to controlled incident irradiance compared with 0.216 and 0.264 kg/m$^3$ day when exposed to a constant incident irradiance of 90 and 165 $\mu mol_{h\nu}/m^2$ s, respectively. These corresponded to areal productivities $P_A$ of 1.63, 1.08, and 1.32 g/m$^2$ day, respectively. This corresponded to a relative increase of 51% and 26% in daily volumetric or areal productivity, respectively. These results demonstrate the advantages of controlling the incident irradiance during microalgae growth in batch mode.

Fig. 5b shows the incident irradiance $G_{in}$ imposed on each face of the PBR as a function of time during the different experiments. It ranged from 120 to 270 $\mu mol_{h\nu}/m^2$ s during the control stage compared with the constant incident irradiance of 90 $\mu mol_{h\nu}/m^2$ s and 165 $\mu mol_{h\nu}/m^2$ s. Note that for $X \geq 1.5$ kg/m$^3$ the concentration signal from the sensor was noisy, as previously discussed. However, it was still used in the feed-forward control as the microalgae were reaching their saturation mass concentration. This resulted in noisy incident irradiance $G_{in}$ estimated using Eq. (12). This issue could be overcome by using an array of sensors operating over complementary concentration ranges (Sandnes et al., 2006). The PAR averaged fluence rate $G_{PAR}(z)$ in the PBR varied by less than 15% with depth for biomass concentration up of 2.5 kg/m$^3$. This observation confirmed the use of the average fluence rate $G_{ave}$ to couple growth rate $\mu$ to the incident irradiance $G_{in}$. Finally, to apply this method of cultivation to PBRs other than flat-plate PBRs, it is necessary to substitute Eq. (3) with the appropriate expression of the fluence rate relevant to the specific PBR geometry. Note however that the validity of the two-flux approximation and Eq. (3) has been established for open ponds and vertical flat-plate PBRs (Lee et al., 2014). In addition, Cornet (2010) derived an analytical expression for the local fluence rate in tubular PBRs, such as those described by Olivieri et al. (2014), based on the two-flux approximation. Alternatively, the RTE can be solved numerically thus removing any restrictions on PBR geometry albeit with added complexity (Lee et al., 2014).

To determine the sensitivity of the feed-forward control scheme, the effects of uncertainty in the measured mass concentration were assessed with respect to the optimum incident irradiance set by the controller and the growth rate of the microorganisms. Underestimating the measured mass concentration of $X = 2$ kg/m$^3$ by 10%, for example, would result in (i) an incident irradiance 6% smaller than its optimum value according to Eq. (12) and (ii) an average fluence rate $G_{ave}$ 6% smaller than the optimum average fluence rate $G_{peak}$. Then using the parabolic relationship obtained between growth rate $\mu$ and $G_{ave}$ (Fig. 4d), the 10% uncertainty in $X$ would result in up to 1.5% decrease in the growth rate $\mu$ relative to its maximum value. This relatively small decrease in growth rate illustrates the robustness of the feed-forward control method proposed in this study.

Fig. 5c shows the growth rate $\mu_{ave}$ as a function of time for the three different experiments. Under constant irradiance

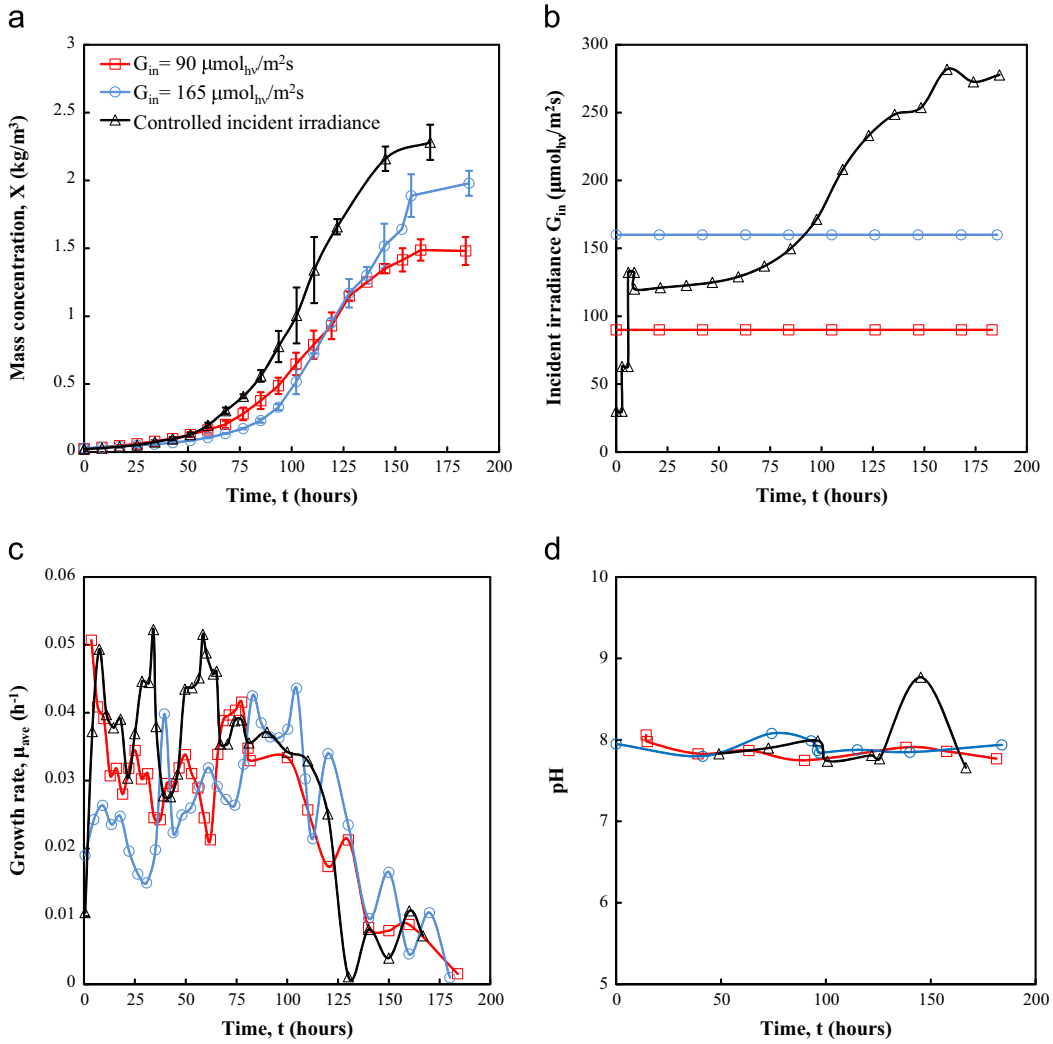


**Fig. 5.** Comparison of the temporal evolution of (a) the mass concentration $X(t)$, (b) the PAR-averaged incident irradiance $G_{in}$ on each face of the PBR, (c) the growth rate $\mu_{ave}(t)$, and (d) the pH of the medium for *N. oculata* grown in flat-plate PBR exposed to controlled or constant incident irradiance of 90 and 165 $\mu mol_{h\nu}/m^2$ s.

$G_{in}$ = 90 $\mu mol_{h\nu}/m^2$ s, the growth rate reached its peak of 0.032 $h^{-1}$ after 1 h and steadily decreased thereafter. On the other hand, under $G_{in}$ = 165 $\mu mol_{h\nu}/m^2$ s the growth rate reached a maximum at 0.042 $h^{-1}$ after approximately 80 h of operation. This was a significantly longer lag time compared with other illumination conditions and was evident in the corresponding mass concentration (Fig. 5a). By contrast, under controlled irradiance, the growth rate fluctuated between 0.05 and 0.03 $h^{-1}$ for up to 120 h of operation. These oscillations could be due to fluctuating pH and dissolved $CO_2$ concentration. In addition, the signal to noise ratio from the mass concentration sensors was too low to accurately estimate the growth rate for concentrations larger than 1.5 $kg/m^3$. Finally, at the end of the growth phase, the nutrients in the medium may have been depleted resulting in nutrient-limited growth conditions leading to a decrease in growth rate that could not be compensated by adjusting the incident light. In fact, nutrient availability in the medium can be estimated by stoichiometric calculation similar to that reported by Kandilian et al. (2013). It was assumed that *N. oculata* cells were elementally composed of 8% nitrogen and 1% phosphate by dry mass (Williams and Laurens, 2010). This suggests that the culture experienced phosphate limitation at a biomass concentration of 1.2 $kg/m^3$ and a nitrogen limitation at around 2.1 $kg/m^3$.

Fig. 5d shows the temporal evolution of the pH of the growth medium averaged between duplicates PBR 1 and PBR 2 and sampled once a day for all experiments. The relative difference in pH between PBR 1 and PBR 2 was negligible at all times. The pH varied between 7.7 and 8.0 and was maintained in the desired range by increasing the $CO_2$ flow rate as the microalgae mass concentration increased. Here, the microalgae *N. oculata* showed the largest growth rate in the 7.7–8.0 range, despite conflicting literature reports (Huertas and Lubián, 1998; Spolaore et al., 2006; Converti et al., 2009; Chiu et al., 2009). Note that no effort was made to continuously maintain a specific pH in the PBR other than daily adjustment of the $CO_2$ flow rate. Nevertheless, further increase in microalgae growth rate could be achieved by applying the same optimal search methodology based on Brent's method to the $CO_2$ concentration and continuously adjusting the $CO_2$ injection rate. Further improvements may also require controlling the dissolved concentrations of individual nutrients in the growth medium to avoid inhibition or limitation by one or several nutrient ingredients.

## 5. Conclusion

This study developed a versatile and general control methodology consisting of (i) a model-free optimal search based on Brent's method and (ii) a feed-forward inversion control of incident irradiance based on continuous mass concentration measurements. For demonstration purposes, marine microalgae *N. oculata* was grown in batch mode in 1 cm thick flat-plate PBRs exposed to

red light from both sides. The optimal search successfully estimated the optimum average fluence rate as 236 $\mu mol_{h\nu}/m^2$ s corresponding to a specific growth rate of 0.06 $h^{-1}$. The microalgae exposed to controlled incident irradiance had a very short lag time and reached saturation mass concentration of 2.25 $kg/m^3$. This should be compared with 1.48 and 2.08 $kg/m^3$ for microalgae grown under 90 and 165 $\mu mol_{h\nu}/m^2$ s, respectively. This corresponded to an average productivity of 0.326 $kg/m^3$ day compared with 0.216 and 0.264 $kg/m^3$ day, respectively. The method demonstrated in this study can be used for any microorganism species and PBR design, as well as for operating parameters other than incident irradiance such as the pH and the medium composition.

## Acknowledgments

This research was supported in part by the U.S. NSF-IGERT program Clean Energy for Green Industry at UCLA (DGE-0903720).

## References

Acien Fernandez, F.G., Garcia Camacho, F., Sanchez Perez, J.A., Fernandez Sevilla, J.M., Molina Grima, E., 1997. A model for light distribution and average solar irradiance inside outdoor tubular photobioreactors for the microalgal mass culture. Biotechnol. Bioeng. 55 (5), 701–714.

Barbosa, M.J., Hoogakker, J., Wijffels, R.H., 2003. Optimisation of cultivation parameters in photobioreactors for microalgae cultivation using the A-stat technique. Biomol. Eng. 20 (4–6), 115–123.

Baroli, I., Melis, A., 1996. Photoinhibition and repair in *Dunaliella salina* acclimated to different growth irradiances. Planta 198, 640–646.

Berberoğlu, H., Pilon, L., 2007. Experimental measurements of the radiation characteristics of *Anabaena variabilis* ATCC 29413-U and *Rhodobacter sphaeroides* ATCC 49419. Int. J. Hydrogen Energy 32 (18), 4772–4785.

Briassoulis, D., Panagakis, P., Chionidis, M., Tzenos, D., Lalos, A., Tsinos, C., Berberidis, K., Jacobsen, A., 2010. An experimental helical-tubular photobioreactor for continuous production of *Nannochloropsis* sp. Bioresour. Technol. 101 (17), 6768–6777.

Carvalho, A., Silva, S., Baptista, J., Malcata, F., 2011. Light requirements in microalgal photobioreactors: an overview of biophotonic aspects. Appl. Microbiol. Biotechnol. 89, 1275–1288.

Chen, C., Yeh, K., Aisyah, R., Lee, D., Chang, J., 2011. Cultivation, photobioreactor design and harvesting of microalgae for biodiesel production: a critical review. Bioresour. Technol. 102(1), 71–81.

Chen, X., Goh, Q.Y., Tan, W., Hossain, I., Chen, W., Lau, R., 2011b. Lumostatic strategy for microalgae cultivation utilizing image analysis and chlorophyll *a* content as design parameters. Bioresour. Technol. 102 (10), 6005–6012.

Chisti, Y., 2007. Biodiesel from microalgae. Biotechnol. Adv. 25 (3), 294–306.

Chisti, Y., 2012. Raceways-based production of algal crude oil. In: Posten, C., Walter, C. (Eds.), Microalgal Biotechnology: Potential and Production. De Gruyter, Berlin, Germany, pp. 113–144.

Chisti, Y., 2013. Constraints to commercialization of algal fuels. J. Biotechnol. 167 (3), 201–214.

Chiu, S., Kao, C., Tsai, M., Ong, S., Chen, C., Lin, C., 2009. Lipid accumulation and $CO_2$ utilization of *Nannochloropsis oculata* in response to $CO_2$ aeration. Bioresour. Technol. 100 (2), 833–838.

Converti, A., Casazza, A.A., Ortiz, E.Y., Perego, P., Borghi, M.D., 2009. Effect of temperature and nitrogen concentration on the growth and lipid content of *Nannochloropsis oculata* and *Chlorella vulgaris* for biodiesel production. Chem. Eng. Process.: Process Intensif. 48 (6), 1146–1151.

Cornet, J.-F., 2010. Calculation of optimal design and ideal productivities of volumetrically lightened photobioreactors using the constructal approach. Chem. Eng. Sci. 65 (2), 985–998.

Cornet, J.-F., Albiol, J., 2000. Modeling photoheterotrophic growth kinetics of *Rhodospirillum rubrum* in rectangular photobioreactors. Biotechnol. Prog. 16 (2), 199–207.

Cornet, J.-F., Dussap, C.-G., 2009. A simple and reliable formula for assessment of maximum volumetric productivities in photobioreactors. Biotechnol. Prog. 25 (2), 424–435.

Cuaresma, M., Janssen, M., van den End, E., Vlchezb, C., Wijffels, R., 2011. Luminostat operation: A tool to maximize microalgae photosynthetic efficiency in photobioreactors during the daily light cycle?. Bioresour. Technol. 102 (17), 7871–7878.

Dauchet, J., Blanco, S., Cornet, J., El Hafi, M., Eymet, V., Fournier, R., 2013. The practice of recent radiative transfer Monte Carlo advances and its contribution to the field of microorganisms cultivation in photobioreactors. J. Quant. Spectrosc. Radiat. Transf. 128, 52–59.

Fernandes, B., Dragone, G., Teixeira, J., Vicente, A., 2010. Light regime characterization in an airlift photobioreactor for production of microalgae with high starch content. Appl. Biochem. Biotechnol. 161 (1–8), 218–226.

Ferrell, J., Sarisky-Reed, V., 2010. National Algal Biofuels Technology Roadmap. Technical Report DOE/EE-0332, Department of Energy, Office of Energy Efficiency and Renewable Energy, Biomass Program, Maryland, Washington DC.

Heng, R.-L., Pilon, L., 2014. Time-dependent radiation characteristics of *Nannochloropsis oculata* during batch culture. J. Quant. Spectrosc. Radiat. Transf. 144, 154–163.

Huertas, I.E., Lubián, L.M., 1998. Comparative study of dissolved inorganic carbon utilization and photosynthetic responses in *Nannochloris* (chlorophyceae) and *Nannochloropsis* (eustigmatophyceae) species. Can. J. Bot. 76 (6), 1104–1108.

IPPC, 2007. Climate Change 2007: Impacts, Adaptation and Vulnerability. Contribution of Working Group II to the Fourth Assessment Report of the Intergovernmental Panel on Climate Change. Cambridge University Press, Cambridge, UK.

Jones, C., Mayfield, S., 2012. Algae biofuels: versatility for the future of bioenergy. Curr. Opin. Biotechnol. 23 (3), 346–351.

Kandilian, R., Lee, E., Pilon, L., 2013. Radiation and optical properties of *Nannochloropsis oculata* grown under different irradiances and spectra. Bioresour. Technol. 137, 63–73.

Kandilian, R., Pruvost, J., Legrand, J., Pilon, L., 2014. Influence of light absorption rate on triglyceride production of *Nannochloropsis oculata*. Bioresour. Technol. 163, 308–319.

Ke, B., 2001. Photosynthesis: Photobiochemistry and Photobiophysics. Advances in Photosynthesis. Kluwer Academic Publishers, Dordrecht, The Netherlands.

Kong, B., Vigil, R.D., 2014. Simulation of photosynthetically active radiation distribution in algal photobioreactors using a multidimensional spectral radiation model. Bioresour. Technol. 158, 141–148.

Lee, E., Pruvost, J., He, X., Munipalli, R., Pilon, L., 2014. Design tool and guidelines for outdoor photobioreactors. Chem. Eng. Sci. 116, 18–29.

McCree, K., 1981. Photosynthetically active radiation. In: Physiological Plant Ecology I: Responses to the Physical Environment, Encyclopedia of Plant Physiology New Series, vol. 12A. Springer-Verlag, Berlin.

Melnicki, M.R., Pinchuk, G.E., Hill, E.A., Kucek, L.A., Stolyar, S.M., Fredrickson, J.K., Konopka, A.E., Beliaev, A.S., 2013. Feedback-controlled LED photobioreactor for photophysiological studies of cyanobacteria. Bioresour. Technol. 134, 127–133.

Modest, M., 2003. Radiative Heat Transfer. Academic Press, San Diego, CA.

Molina Grima, E., Fernandez Sevilla, J.M., Sanchez Perez, J.A., Garcia Camacho, F., 1996. A study on simultaneous photolimitation and photoinhibition in dense microalgal cultures taking into account incident and averaged irradiances. J. Biotechnol. 45 (1), 59–69.

Murphy, T., Berberoğlu, H., 2011. Effect of algae pigmentation on photobioreactor productivity and scale-up: a light transfer perspective. J. Quant. Spectrosc. Radiat. Transf. 112 (18), 2826–2834.

Neidhardt, J., Benemann, J.R., Zhang, L., Melis, A., 1998. Photosystem-II repair and chloroplast recovery from irradiance stress: relationship between chronic photoinhibition, light-harvesting chlorophyll antenna size and photosynthetic productivity in *Dunaliella salina* (green algae). Photosynth. Res. 56, 175–184.

Olivieri, G., Salatino, P., Marzocchella, A., 2014. Advances in photobioreactors for intensive microalgal production: configurations, operating strategies and applications. J. Chem. Technol. Biotechnol. 89 (2), 178–195.

Pilon, L., Berberoğlu, H., Kandilian, R., 2011. Radiation transfer in photobiological carbon dioxide fixation and fuel production by microalgae. J. Quant. Spectrosc. Radiat. Transf. 112 (17), 2639–2660.

Pottier, L., Pruvost, J., Deremetz, J., Cornet, J., Legrand, J., Dussap, C., 2005. A fully predictive model for one-dimensional light attenuation by *Chlamydomonas reinhardtii* in a torus photobioreactor. Biotechnol. Bioeng. 91 (5), 569–582.

Press, W., Teukolsky, S.A., Vetterling, W.T., Flannery, B.P., 2007. Numerical Recipes: The Art of Scientific Computing. Cambridge University Press, New York, NY.

Pruvost, J., Cornet, J., 2012. Knowledge models for the engineering and optimization of photobioreactors. In: Posten, C., Walter, C. (Eds.), Microalgal Biotechnology: Potential and Production. De Gruyter, Berlin, Germany, pp. 181–224.

Sandnes, J., Ringstad, T., Wenner, D., Heyerdahl, P., Kllqvist, T., Gislerd, H., 2006. Real-time monitoring and automatic density control of large-scale microalgal cultures using near infrared (NIR) optical density sensors. J. Biotechnol. 122 (2), 209–215.

Spolaore, P., Joannis-Cassan, C., Duran, E., Isambert, A., 2006. Optimization of *Nannochloropsis oculata* growth using the response surface method. J. Chem. Technol. Biotechnol. 81 (6), 1049–1056.

Stephens, E., Ross, I., King, Z., Mussgnug, J., Kruse, O., Posten, C., Borowitzka, M., Hankamer, B., 2010. An economic and technical evaluation of microalgal biofuels. Nat. Biotechnol. 28 (2), 126–128.

Sukenik, A., Levy, R., Levy, Y., Falkowski, P., Dubinsky, Z., 1991. Optimizing algal biomass production in an outdoor pond: a simulation model. J. Appl. Phycol. 3, 191–201.

Svrcek, W., Mahoney, D., Young, B., 2007. Advanced Topics in Classical Automatic Control. John Wiley & Sons, Ltd, New York, NY, pp. 131–146.

Takache, H., Pruvost, J., Cornet, J.-F., 2012. Kinetic modeling of the photosynthetic growth of *Chlamydomonas reinhardtii* in a photobioreactor. Biotechnol. Prog. 28 (3), 681–692.

Van Vooren, G., Grand, F.L., Legrand, J., Cuine, S., Peltier, G., Pruvost, J., 2012. Investigation of fatty acids accumulation in *Nannochloropsis oculata* for biodiesel application. Bioresour. Technol. 124, 421–432.

Williams, P.J., Laurens, L., 2010. Microalgae as biodiesel and biomass feedstocks: review and analysis of the biochemistry, energetics and economics. Energy Environ. Sci. 3, 554–590.